Atomic fine-structure lines in the ISO-SWS spectra of the supergiants alpha Orionis and alpha Scorpii

Justtanont, K.; Tielens, A.G.G.M.; de Jong, T.; Cami, J.; Waters, L.B.F.M.; Yamamura, I.

ASTRONOMY
AND
ASTROPHYSICS

Atomic fine-structure lines in the ISO-SWS spectra
of the supergiants α Orionis and α Scorpii[*]

K. Justtanont[1], A.G.G.M. Tielens[2,3], T. de Jong[4,5], J. Cami[2,5], L.B.F.M. Waters[5,2], and I. Yamamura[5]

[1] Stockholm Observatory, S-133 36 Saltsjöbaden, Sweden
[2] SRON-Groningen, P.O.Box 800, 9700 AV Groningen, The Netherlands
[3] Kapteyn Institute, P.O.Box 800, 9700 AV Groningen, The Netherlands
[4] SRON-Utrecht, Sorbonnelaan 2, 3584 CA Utrecht, The Netherlands
[5] Astronomical Institute 'Anton Pannekoek', University of Amsterdam, Kruislaan 403, 1098 SJ Amsterdam, The Netherlands

Abstract. We report the detection of infrared fine-structure lines of [Fe II] and [Si II] in the ISO-SWS spectra of two supergiants, α Ori and α Sco. From the observed intensities we infer that the emitting regions have temperatures in the range 1200–1800 K and are located within about 20 R_* from the star. This is interior to the region where dust is supposed to condense in the expanding envelope so that Fe and Si are not yet incorporated into the dust. The gas density required to thermalize these lines is of order 10^6 cm^{-3} consistent with the expected density in the outflow at the adopted location. The total mass of gas being cooled through these atomic fine structure lines is of the order of 10^{-4} M$_\odot$. Our calculation shows that cooling through the [O I] 63 μm line extends over a larger radius than for both [Fe II] and [Si II].

Key words: stars: chromospheres – stars: circumstellar matter – stars: individual: α Ori – stars: individual: α Sco – stars: late-type – infrared: stars

1. Introduction

The thermal balance of the gas in circumstellar envelopes of red giants has been studied extensively, both theoretically and observationally. In an early study of OH/IR stars Goldreich & Scoville (1976) concluded that the gas is predominantly heated by friction between radiatively driven dust and gas and cooled by molecular line radiation, chiefly from H_2O and CO. In the case of supergiants the situation is complicated by the fact that the mass loss rate is usually a few orders of magnitude smaller than for OH/IR stars and by the presence of a chromosphere which can lead to photoionization and dissociation of atoms and molecules close to the photosphere.

A detailed model of α Ori has been proposed by Rodgers & Glassgold (1991, hereafter RG) who calculated the gas kinetic temperature from the energy balance equation, taking into account heating via gas-grain collision, photoelectric heating by dust grains in the outer envelope and radiative cooling via atomic fine-structure lines and molecular transitions. They found that the latter are unimportant in the circumstellar envelope of α Ori because of the low abundances of CO and H_2O. The main cooling line is the [O I] 63 μm line.
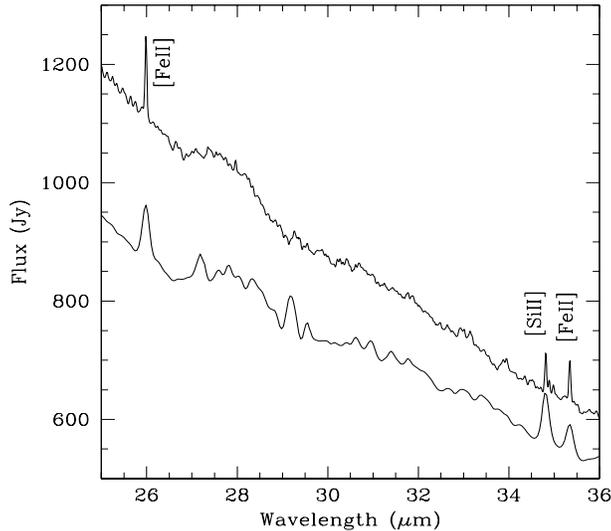
Observations of atomic fine-structure lines are hampered by absorption in the earth atmosphere. Using the Kuiper Airborne Observatory (KAO) Haas et al. (1995, hereafter HGT, see also Erikson et al. 1995) observed a number of supergiants in [O I] at 63 and 146 μm and in [Si II] at 35 μm. All stars in their sample were detected in the [O I] line. Only two stars were detected in the [Si II] line, α Sco and α Ori. Recently, detection of atomic fine-structure lines has been reported in the ISO-SWS spectra of AGB stars by Aoki et al. (1998).

In this paper we present ISO-SWS spectra of the supergiants α Ori and α Sco along with results of modelling the spectral energy distributions (SED). Three fine-structure lines are detected in our spectra, identified with transitions of the ions [Fe II] and [Si II]. We investigate where these lines originate using the model of RG.

2. Observations

For both supergiants in our sample, we have full-grating ISO/SWS spectra with a complete wavelength coverage from 2–45 μm (AOT01). We obtained a fast scan for α Sco (speed 1, resolution of 250) and a slow scan for α Ori (speed 4, resolution about 1000).

The data were reduced using the SWS Interactive Analysis (SIA) reduction software package using standard ISO pipeline data products (version 6.0) at the data centre in Groningen. Although in principle flux levels may be affected by the uncertainty in the dark current the high flux levels of our stars ensure that this effect can be neglected here. The main uncertainty in the observed flux comes from the pointing uncertainty and the

Fig. 1. Grating spectra of α Ori (*top*) and α Sco (*bottom*) showing the three atomic fine-structure lines. Note that the flux for α Sco has been multiplied by 1.6 in this plot.

Table 1. Observed line fluxes and the critical densities.

Species	wavelength (μm)	Line flux (W cm^{-2}) α Ori	α Sco	n_{cr}^{b} cm^{-3}
[Fe II]	25.99	2.8E-18	4.4E-18	2.2E+6
[Fe II]	35.35	8.1E-19	1.4E-18	3.3E+6
[Si II]	34.81	7.2E-19	2.5E-18	3.4E+5
[O I][a]	63.18	1.1E-18	2.0E-18	4.7E+5
[O I][a]	145.5	1.1E-19	–	9.5E+4

[a] fluxes taken from HGT
[b] values taken from Tielens & Hollenbach (1985)

Fig. 2. The fits to SED of α Ori (*top*) and α Sco (*bottom*). Note that the spectrum of α Sco is shifted down by a factor of 10 in this plot. Crosses are the observed ISO SWS spectra; open circles are photometry from Low et al. (1970) and Epchtein et al. (1980); filled squares are IRAS photometry.

Table 2. Parameters of SED modelling

	α Ori	α Sco
Stellar effective temperature (K)	3600	3300
Stellar radius (cm)	6.5E13	6.1E13
Dust condensation radius (cm)	1.5E15	1.6E15
Terminal velocity (km s^{-1})	16	17
Distance (pc)	200	180
Dust mass loss rate (M$_{\odot}$ yr^{-1})	9.0E-10	6.0E-10

relative spectral response function (RSRF). A bump at 28 μm in Fig. 1 may be spurious, due to instrumental effects in band 3E between 27.5 and 29 μm. Spectra of both supergiants are presented in Fig. 1 and line fluxes are given in Table 1.

3. Modelling the IR energy distribution

We have modelled the spectral energy distribution (SED) of the two stars. The calculational procedure is described in Haisch (1979) and Justtanont & Tielens (1992). We assume a spherical symmetry with a constant mass loss rate. The grain size distribution used is that for the interstellar grain size distribution (Mathis, Rumpl, Nordsieck 1977). The calculation takes into account the thermal emission and multiple scattering due to silicate grains. Adopted and derived parameters are listed in Table 2.

The parameters derived for α Ori from fitting the SED (Table 2) are quite similar to those derived by Skinner & Whitmore (1987) who also considered the effects of the chromosphere of the star. The values for the stellar radius and effective temperature also agree with interferometric observations by Dyck et al. (1996). The inner radius of the dust shell is taken from Skinner

et al. (1997) to be 0''.5 rather than 0''.9 based on the 11 μm interferometry by Bester et al. (1991). The model fit to the SWS observation, along with the ground based photometry fluxes are shown in Fig. 2. We estimated a dust mass loss rate of 9×10^{-10} M$_{\odot}$ yr^{-1} from our model fit. The dust mass loss rate used in RG model is very similar to this. It is an important parameter in calculating the dust-drag heating which is the main heating source in the circumstellar envelope of α Ori.

Occultation observation of α Sco gives an estimate of the stellar radius of 22.83 mas, i.e., 6.1×10^{13} cm at a distance of 180 pc (Dyck et al. 1996). Bloemhof & Danen (1995) measured the inner radius of the dust shell to be 0.''6, i.e., 1.6×10^{15} cm at 180 pc. The fit to the SED is shown in Fig. 2 with the model parameters in Table 2. Both supergiants have very similar input parameters. They also have similar derived dust mass loss rates which are very low, as reflected by their weak 10 μm silicate feature.

4. Atomic fine structure lines

Our SWS full-grating spectra of the supergiants α Sco and α Ori show strong atomic fine-structure lines of two species, [Fe

II] at 25.99 and 35.35 μm and [Si II] at 34.81 μm (Fig. 1). We list the line fluxes in Table 1.

The two [Fe II] lines originate in the same ladder connecting the three lowest fine-structure levels of the a^6D state. The line at 25.99 μm is from the J=7/2 to the J=9/2 (ground) state while the 35.35 μm line is between the J=5/2 and 7/2 state. The ratio of the line fluxes is then a good temperature indicator. The line intensity, for the optically thin case, can be calculated from

$$I_{ji} = N_j \frac{h\nu_{ij}A_{ji}}{4\pi} \qquad (1)$$

where N_j is the column density of the upper (j) level, ν_{ij} is the transition frequency between levels (j) and (i), and A_{ji} is the Einstein A coefficient for spontaneous emission. For the [Fe II] lines, assuming that both arise in the same region, we can calculate the excitation temperature, T, of the emitting gas from the ratio of the populations in the levels J=5/2 and J=7/2 using the expression

$$\frac{N_j(T)}{N_i(T)} = \frac{g_j}{g_i} exp(-h\nu_{ij}/kT) \qquad (2)$$

where g_i is the statistical weight of level i.

4.1. α Ori

The supergiant α Ori has been extensively studied from the KAO in the atomic fine-structure lines. It is known that the line intensity of the [O I] 63 μm line varies with time (HGT), corresponding to the variation in the V band with an amplitude of about 0.25 magnitude (Krisciunas 1992, 1994). Our observed line flux in the [Si II] line agrees reasonably well with that observed by HGT.

We measure the line fluxes of the two [Fe II] lines and these are listed in Table 1. Directly from the ratio of the [Fe II] 26 to 35 μm line fluxes, we can calculate the excitation temperature of the gas and estimate the total numer of atoms involved in the cooling process in the circumstellar envelope, independent of model assumption which we will later investigate. The line flux ratio is 3.43 which translates to a ratio of the column densities of the J=5/2 to J=7/2 levels of 0.54. Using Eq. 2, we obtain a temperature of 1230 K. The assumption made here is that the emission is optically thin; hence, we see all the emitting atoms. The numbers of atoms in the upper levels (N_j) is listed in Table 3. They can be converted to the total mass of gas, assuming an excitation temperature of 1230 K and assuming the solar abundance for Si (3.8×10^{-5}), and Fe (3.4×10^{-5}), and using the measured O abundance for α Ori from Lambert et al. (1984) of 5.9×10^{-4}. The average mass of the gas cooling through these atomic fine structure lines derived from our observations are in reasonable agreement, of the order of 10^{-4} M$_\odot$. At this temperature, the emission originates inside the dust forming region since the condensation temperature for silicate is 1000 K, and probably arises in the chromospheric region of the star.

Our observations can also be compared to the detailed model developed for α Ori by RG. The line fluxes predicted by this model are given by
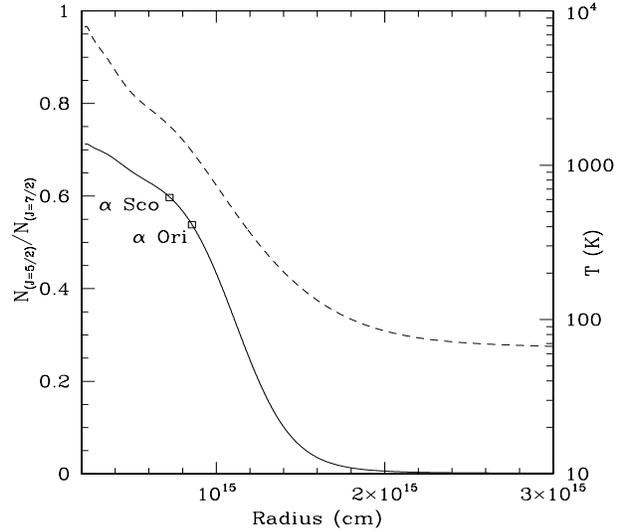
Fig. 3. The ratio of the populations of [FeII] (solid line) as calculated from Eq. 2 assuming RG temperature distribution (dashed line). Also marked are the results from our observations using Eq. 2.

Table 3. The total number of atoms in the upper level (N_j) calculated from the line fluxes and their corresponding gas mass (see text for details).

| Species	α Ori		α Sco	
	N_j	M_H (M$_\odot$)	N_j	M_H (M$_\odot$)
[Fe II] 26	8.2E47	7.1E-5	9.3E47	7.5E-5
[Fe II] 35	4.4E47	7.1E-5	5.5E47	7.5E-5
[Si II] 35	2.8E48	1.1E-4	7.1E48	2.6E-4
[O I] 63	1.9E47	8.8E-5	2.5E48	1.3E-4

$$F_{ji} = \frac{\dot{M}x_0 A_{ji}h\nu_{ji}}{4\pi \ m_H v D^2} \int P_j(r)dr \qquad (3)$$

where $\dot{M}$ is the gas mass loss rate, D is the distance to the star, x_0 is the abundance of element x and $P_j(r)$ is the fractional abundance of level j at radius r. Fig. 3 shows the temperature structure of the RG model, and also indicate the ratio of the [Fe II] populations calculated from the model. The [Fe II] ratio equals the observed ratio at a radius of 8.5×10^{14} cm. Fig. 4 shows the fractional population of the upper levels of [Fe II], [Si II] and [O I].

We calculate the total number of emitting atoms of all the species observed, interior to the emitting region which produce the observed line fluxes. The normalised populations of the upper level of each transition for each species are used to calculate the flux in Eq. 3. HGT assumed a mass loss rate of 4×10^{-6} M$_\odot$ yr^{-1} and a constant velocity of 16 km s^{-1} within a radius of 3×10^{15} cm in order to match their observed fluxes of [O I] and [Si II] lines. The derived fluxes depend directly on the mass loss rate assumed. The estimated gas mass loss rate for α Ori ranges between 2–4×10^{-6} M$_\odot$ yr^{-1}, as measured by the [C I] line (Huggins et al. 1994, van der Veen et al. 1999) and by [K I] scattering observation (Mauron et al. 1984). Here, we will use a value of 4×10^{-6} M$_\odot$ yr^{-1} for the subsequent line flux calcu-
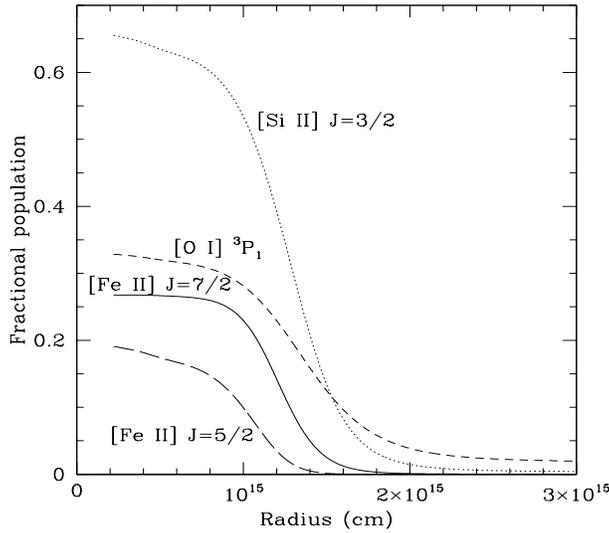
Fig. 4. Fraction population of [Si II] J=3/2, [Fe II] J=5/2, J=7/2, and [O I] $^3P_1$ as a function of radius, assuming the temperature distribution from RG.
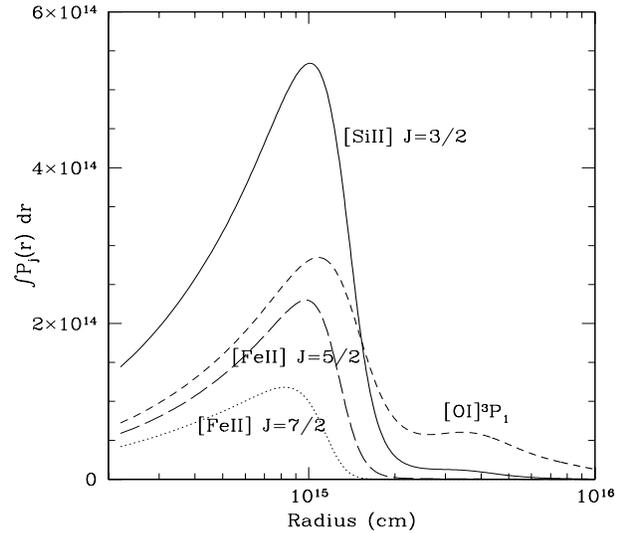
Fig. 5. Contribution to the emission line fluxes for each species as a function of radius. Note that for [O I]$^3P_1$, there is a significant contribution from the outer part of the envelope.

Table 4. Calculated model line flux based on RG's model

| Species | Line fluxes (W cm^{-2}) | |
	α Ori	α Sco
[Fe II] 26	2.9E-18	5.4E-18
[Fe II] 35	8.4E-19	1.6E-19
[Si II] 35	6.2E-19	1.2E-18
[O I] 63	1.3E-18	2.5E-18
[O I] 146	3.0E-20	5.5E-20

lation and assume RG temperature profile for the star. We can directly compare predicted fluxes from RG with the observations (Table 4 in RG). Their model predicts line fluxes for [Si II] and [O I] which are very close to the observed values. Here, we include [Fe II] in their model and the results are listed in Table 4 (see Table 1 for observed line fluxes) which show excellent agreement between the model results and the observations.

Fig. 5 shows the integrated population of the upper levels of different atomic species investigated here (Eq. 3) which shows where the flux of each line arises. We note here that although the bulk of the flux for the [O I] 63 μm line originate from within 1.5×10^{15} cm, there is about 25% of emission coming from beyond this radius. This is due to the slow decline of the relative population of oxygen as a function of radius, assuming the RG temperature profile (Fig. 4). As previously discussed, the predicted line fluxes agree very well with the observed ones. However, the calculated 63/146 μm [O I] flux ratio is much higher than observed by HGT, 40 vs. 10 although it is worthy to note here that the 146 μm line is a 2.5-sigma detection only. Recently, Barlow (1999) reported a line flux for [O I] 146 μm of about 4×10^{-20} W cm^{-2}. This large 63/146 μm flux ratio may be due to the 63 μm being optically thick (Tielens & Hollenbach 1985) while the 146 μm is optically thin hence the assumption of Eq. 1 then breaks down.

The model calculation implicitly assumes that all Fe is singly ionized. The energy requires to ionize Fe I to Fe II is 8.1 eV while to ionize it further requires a very high energy of 16.2 eV. The expected [Fe III] lines at 13.53 and 22.93 μm are not seen in the spectrum. The relatively strong UV radiation from the chromosphere should ensure that the atoms remain singly ionize. The same argument applies for Si since its ionization energies are very similar to those for Fe. From the model calculation, we estimate the total mass of the emitting gas within the radius of 3×10^{15} cm to be 1.2×10^{-4} M$_\odot$, slightly higher than obtained from simple LTE estimate from Table 2. Note that for the [O I] $^3P_1$, the mass outside this may provide some contribution to the observed flux (Fig. 5). The excitation energy for this level is 228 K hence it does not require high gas temperature to excite it up to the $^3P_1$ level.

The mass loss rates derived from the atomic fine structure lines of [O I], [Si II], and [Fe II] are in seemingly good agreement with those obtained from [C I] emission and [K I] scattering (van der Veen et al. 1999; Mauron et al. 1984). However, our data really measure a total mass of emitting gas and this gas is located within the dust condensation radius. Hence, actually, a much lower flow velocity (~ 2 km s^{-1}; Habing et al. 1994) should be used to calculate the mass loss rate from these data than adopted by RG (16 km s^{-1}). As a result the mass loss rate calculated near the stellar surface is only 5×10^{-7} M$_\odot$ yr^{-1}; a factor 4–8 less than from the [C I] and [K I] data for the outer envelope. Evidence for variable mass loss (i.e., discrete dust mass loss events of modest size) have been reported by Bester et al. (1996) in their 11 μm interferometric study of the dust emission. It seems therefore that, compared to the mass loss measured in [C I] and [K I], we have caught α Ori in a quiescent episode. With either mass loss rate, the density inside the dust condensation radius is well above the critical densities for all species (Table 1). It is interesting to note the very high gas-to-dust mass ratio of ≥ 550 which is much higher than 160,

suggested by Knapp (1985) for AGB stars. The presence of the chromosphere around α Ori may inhibit grain formation thereby resulting in such a low dust mass loss rate compared to the gas mass loss rate.

4.2. α Sco

This star is known to have a B2 companion which is only $3''$ from the supergiant, α Sco A (Hjellming & Newell 1983). The source of ionizing photons may originate from both the chromosphere, as for the case of α Ori, as well as from the hot companion. The large aperture size of SWS ($14'' \times 20''$) also ensures that both stars are present in the beam.

Following a similar approach we took for α Ori, the ratio of the column density of the [Fe II] J=5/2 to J=7/2 is 0.60. Using Eq. 2, this leads to a temperature of the emitting region for [Fe II] of 1785 K, slightly hotter than for α Ori. The total number of emitting atoms and the corresponding hydrogen masses derived from the observed line fluxes are listed in Table 3. The average mass of the gas from all lines considered is 1.3×10^{-4} M$_\odot$. We note that the [Si II]/[Fe II] 35 μm ratio is a factor of two larger in this star than in α Ori.

We calculate the expected line fluxes using Eq. 3 and integrate the flux within the dust condensation radius of 3×10^{15} cm. We obtained line fluxes close to those observed (Table 4), using a gas mass loss rate of 6.4×10^{-6} M$_\odot$ yr^{-1} and a constant velocity of $17\,\mathrm{km\,s^{-1}}$ (Bernat 1982). Here, we assume the same abundances of all the elements considered to be the same as for α Ori and also using the same gas temperature distribution.

From the derived excitation of the [Fe II] flux ratio, the emission comes from within the dust condensation radius. This is also supported by RG's temperature (Fig. 3). This may have a similar implication as for α Ori case that the wind in this region has not yet reached the terminal velocity of $17\,\mathrm{km\,s^{-1}}$.

Finally, we determined the gas mass within the emitting region from fitting the observed line fluxes using Eq. 3 to be 1.7×10^{-4} M$_\odot$. This value is comparable to the average derived from Table 2. Bernat (1982) quoted a gas mass loss rate of 6.4×10^{-6} M$_\odot$ yr^{-1} but with a large spread of $(0.38$–$10)\times10^{-6}$ M$_\odot$ yr^{-1}. Our derived dust mass loss rate for α Sco is 6×10^{-10} M$_\odot$ yr^{-1} hence the deduced gas-to-dust mass ratio is very large (≥ 600), making it one of the highest gas-to-dust mass ratio. As we noted earlier, the system is complicated by a presence of the B2 companion. Hjellming & Newell (1983) detected radio emission around the companion. UV observations also suggest that the companion is a source of ionizing Fe III line, not seen in α Ori (van der Hucht et al. 1979). It is possible that both the chromosphere of the supergiant and the intense radiation from the companion disrupts the dust formation process, or destroys dust grains in the supergiant wind.

5. Summary

From the fluxes of atomic fine structure lines observed in the SWS spectra of α Ori and α Sco, we can deduce the temperature of the emitting regions to be 1230 and 1785 K, respectively.

Both stars have similar outflow velocities hence the radii of the emitting gas are about the same, 20 R$_*$, assuming that both have similar temperature structures in the inner part. This region of the envelope is just inside the dust forming region as seen from interferometry from the radio and infrared (Bester et al. 1991; Skinner et al. 1997). From the mass loss rates, the emitting regions of both stars have density above the critical density to thermalize both [Fe II] and [Si II] lines. In both stars, the source of the UV photons which ionize these observed lines is their chromospheres. In α Sco, where the highest ratio of Si [II]/Fe [II] lines is observed, the abundance of Si may be higher than in α Ori. We also find that there is contribution from [O I] line fluxes exterior to the emitting region of [Fe II] and [Si II], although most of the fluxes come from this same region.

The masses of gas which cooled via the atomic fine structure lines in both supergiants are very comparable and are of the order of 10^{-4} M$_\odot$. The derived mass loss rate of this region, assuming a thermal velocity of $2\,\mathrm{km\,s^{-1}}$ is $\sim 6\times10^{-7}$ M$_\odot$ yr^{-1}. The gas-to-dust mass ratio of both stars are much higher than observed in AGB stars.

References

Aoki W., Tsuji T., Ohnaka K., 1998, A&A, in press
Barlow M.J., 1999, In: Le Bertre T., Waelkens C., Lèbre A. (eds.) IAU Symp. 191 AGB Stars, in press
Bernat A.P., 1982, ApJ 252, 644
Bester M., Danchi W.C., Degiacomi C.G., Townes C.H., Geballe T.R., 1991, ApJ 367, L27
Bester M., Danchi W.C., Hale D., et al., 1996, ApJ 463, 336
Bloemhof E.E., Danen R.M., 1995, ApJ 440, L93
Dyck H.M., Bensen J.A., van Belle G.T., Ridgway S.T., 1996, AJ 111, 1705
Erikson E.F., Haas M.R., Colgan S.W.J., Simpson J.P., Rubin R.H., 1995, In: Haas M.R., Davidson J.A. (eds.) Airborne Astronomy Symposium on the galactic ecosystem: from gas to stars to dust. ASP, San Francisco, p. 523
Epchtein N., Guibert J., Nguyen-Q-Rieu, Turon P., Wamsteker W., 1980, A&A 85, L1
Goldreich P., Scoville N., 1976, ApJ 205, 144
Haas M.R., Glassgold A.E., Tielens A.G.G.M., 1995, In: Haas M.R., Davidson J.A. (eds.) Airborne Astronomy Symposium on the galactic ecosystem: from gas to stars to dust. ASP, San Francisco, p. 397 (HGT)
Haisch B.M., 1979, A&A 72, 161
Habing H., Tignon J., Tielens A.G.G.M., 1994, A&A 286, 523
Hjellming R.M., Newell R.T., 1983, ApJ 275, 704
Huggins P.J., Bachiller R., Cox P., Forveille T., 1994, A&A 424, L127
Justtanont K., Tielens A.G.G.M., 1992, ApJ 389, 400
Knapp G.R., 1985, ApJ 293, 273
Krisciunas K., 1992, IAU Inform. Bull. on Variable Stars No. 3728
Krisciunas K., 1994, IAU Inform. Bull. on Variable Stars No. 4028
Lambert D.L., Brown J.A., Hinkle K.H., Johnson H.R., 1984, ApJ 284, 233
Low F.J., Kleimann D.E., Latham A.S., Geisel S.J., 1970, ApJ 160, 531

Mathis J.S., Rumpl W., Nordsieck K.H., 1977, ApJ 217, 425

Mauron N., Fort B., Querci F., et al., 1984, A&A 130, 341

Rodgers B., Glassgold A.E., 1991, ApJ 382, 606 (RG)

Skinner C.J., Dougherty S.M., Meixner M., et al., 1997, MNRAS 288, 295

Skinner C.J., Whitmore B., 1987, MNRAS 224, 335

Tielens A.G.G.M., Hollenbach D.J., 1985, ApJ 291, 722

van der Hucht K.A., Stencel R.E., Haisch B.M., Kondo Y., 1979, A&AS 36, 377

van der Veen W.E.C.J., Huggins P.J., Matthews H.E., 1999, in press